AGU PUBLICATIONS

Water Resources Research

RESEARCH ARTICLE
10.1002/2014WR015811

Key Points:
- Heterogeneity and viscous fingering both impact fluid mixing in porous media
- We identify the physical mechanisms that control breakthrough and removal times
- We elucidate the structural and hydrodynamic contributions to rate of mixing

Correspondence to:
R. Juanes,
juanes@mit.edu

Citation:
Nicolaides, C., B. Jha, L. Cueto-Felgueroso, and R. Juanes (2015), Impact of viscous fingering and permeability heterogeneity on fluid mixing in porous media, *Water Resour. Res.*, *51*, doi:10.1002/2014WR015811.

Received 15 MAY 2014
Accepted 8 MAR 2015
Accepted article online 16 MAR 2015

© 2015. American Geophysical Union. All Rights Reserved.

Impact of viscous fingering and permeability heterogeneity on fluid mixing in porous media

Christos Nicolaides[1], Birendra Jha[1], Luis Cueto-Felgueroso[1,2], and Ruben Juanes[1]

[1]Department of Civil and Environmental Engineering, Massachusetts Institute of Technology, Cambridge, Massachusetts, USA, [2]Civil Engineering School, Technical University of Madrid, Madrid, Spain

Abstract Fluid mixing plays a fundamental role in many natural and engineered processes, including groundwater flows in porous media, enhanced oil recovery, and microfluidic lab-on-a-chip systems. Recent developments have explored the effect of viscosity contrast on mixing, suggesting that the unstable displacement of fluids with different viscosities, or viscous fingering, provides a powerful mechanism to increase fluid-fluid interfacial area and enhance mixing. However, existing studies have not incorporated the effect of medium heterogeneity on the mixing rate. Here, we characterize the evolution of mixing between two fluids of different viscosity in heterogeneous porous media. We focus on a practical scenario of divergent-convergent flow in a quarter five spot geometry prototypical of well-driven groundwater flows. We study by means of numerical simulations the impact of permeability heterogeneity and viscosity contrast on the breakthrough curves and mixing efficiency, and we rationalize the nontrivial mixing behavior that emerges from the competition between the creation of fluid-fluid interfacial area and channeling.

1. Introduction

Spatial variation in rock properties such as porosity and permeability leads to first-order effects in macroscopic flow and transport through geologic formations [*Bear*, 1972; *Dagan*, 1989; *Gelhar*, 1993]. The effect of permeability heterogeneity on macrodispersion and *spreading* of passive tracers has been extensively studied in groundwater hydrology for many decades [*Rubin*, 2003; *Kitanidis*, 1988; *Zhang and Neuman*, 1990; *Berkowitz et al.*, 2006]. Recently, the topic of flow and transport through heterogeneous media has received increasing attention due to the need to better quantify *mixing* (as opposed to spreading), as it plays a critical role in subsurface chemical reactions [*Le Borgne et al.*, 2008; *Cirpka et al.*, 2008; *Tartakovsky et al.*, 2009; *Le Borgne et al.*, 2010; *Jha et al.*, 2011a; *Dentz et al.*, 2011; *Chiogna et al.*, 2012; *Jha et al.*, 2013; *de Anna et al.*, 2013].

In addition to spatial variation in rock properties, the physical properties of a groundwater contaminant can also vary in space and time due to nonlinear dependence of its density, viscosity, and diffusivity on the concentrations of the dissolved species [*Flowers and Hunt*, 2007]. A contaminant can be more viscous than the ambient fluid, e.g., plumes of nonhalogenated semivolatile compounds (m-Cresol, dibutyl phthalate), halogenated volatiles (ethylene dibromide), jet fuel, and fuel oil in an aquifer, or it can be less viscous, e.g., halogenated volatiles (trichloroethane, methylene chloride, dichloroethylene, chloroform), gasoline, alcohols, and ethers (methyl tertiary butyl ether or MTBE) [*Boulding*, 1996]. Further, the viscosity may change with time due to phase separation, dissolution, and evaporation of lighter volatile components [*Mercer and Cohen*, 1990].

In the context of subsurface flow and transport, it is well known that the displacement of a more viscous fluid by a less viscous one leads to a hydrodynamic instability known as viscous fingering [*Bensimon et al.*, 1986; *Homsy*, 1987]. Most contaminants are partially soluble in water, with solubility depending on the pH as well as on the presence of any cosolvents, which can increase the solubility dramatically [*Fu and Luthy*, 1986; *Boulding*, 1996]. Treatment of NAPLs (non-aqueous phase liquids) with surfactants can also produce contaminant plumes where the viscosity contrast between the plume and the ambient water depends on dissolved concentrations of the contaminant [*Dwarakanath et al.*, 1999; *Mulligan et al.*, 2001]. The effect of viscous fingering on spreading and mixing of slugs of fluid in a porous medium or a Hele-Shaw cell has been studied through laboratory experiments [*Kopf-Sill and Homsy*, 1988; *Bacri et al.*, 1992; *Petitjeans et al.*,

1999; *Held and Illangasekare*, 1995; *Christie et al*., 1990; *Davies et al*., 1991] and numerical simulations [*Christie and Bond*, 1987; *Tan and Homsy*, 1988; *Christie*, 1989; *Zimmerman and Homsy*, 1991, 1992a; *De Wit et al*., 2005; *Mishra et al*., 2008; *Jha et al*., 2011a, 2011b, 2013]. A number of experimental, theoretical, and numerical studies have been carried out to understand the effects of anisotropic dispersion [*Yortsos and Zeybek*, 1988; *Zimmerman and Homsy*, 1991, 1992b], gravity [*Tchelepi and Orr*, 1994; *Manickam and Homsy*, 1995; *Lajeunesse et al*., 1997; *Ruith and Meiburg*, 2000; *Fernandez et al*., 2002; *Riaz and Meiburg*, 2003], chemical reactions [*Fernandez and Homsy*, 2003; *De Wit and Homsy*, 1999; *De Wit*, 2001; *Nagatsu et al*., 2007], adsorption [*Mishra et al*., 2007], and flow configuration [*Paterson*, 1985; *Zhang et al*., 1997; *Chen and Meiburg*, 1998a, 1998b; *Pritchard*, 2004; *Chen et al*., 2008] on viscous fingering. The effect of mild levels of heterogeneity (variance of log-permeability field less than one) on *spreading* of slugs due to viscous fingering has also been studied [*Welty and Gelhar*, 1991; *Tan and Homsy*, 1992; *Tchelepi et al*., 1993; *De Wit and Homsy*, 1997a, 1997b; *Chen and Meiburg*, 1998b; *Kempers and Haas*, 1994; *Sajjadi and Azaiez*, 2013]. However, the evolution of *mixing* and *dilution* during viscously unstable flow in strongly heterogeneous media remains unexplored.

In this paper, we revisit the problem of subsurface contaminant transport through a heterogeneous aquifer and we focus on the impact of two principal sources of disorder in the flow field: viscosity contrast between the fluids and heterogeneity in the permeability field. We consider a wide range of viscosity ratios of the contaminant and the water, from a less viscous to a more viscous contaminant, flowing through a range of permeability fields, from almost homogeneous to strongly heterogeneous. We ask the following practical question: how does the interplay between viscosity contrast and permeability heterogeneity determine the evolution of macroscopic quantities that characterize the spatial structure and temporal evolution of a contaminant plume? We answer this question by conducting high-resolution simulations of contaminant flow and transport in an aquifer, and by analyzing both point measurements of contaminant breakthrough and clean-up times as well as global degree of mixing and dilution of the contaminant plume.

In previous studies of contaminant transport in heterogeneous media, the focus has primarily been on modeling rectilinear flow through a vertical cross-section of the aquifer with a line source injection. These conditions are favorable for estimating vertical sweep efficiency of the contaminant displacement process [*Tchelepi et al*., 1993; *Le Borgne et al*., 2008]. In this study, we use the quarter five spot displacement pattern as our flow configuration where the contaminant transport is driven by fluid injection and extraction at wells [*Cortis et al*., 2004; *Berkowitz et al*., 2006]. The quarter five spot pattern is a canonical configuration for characterizing areal sweep efficiency during enhanced oil recovery by waterflooding or CO_2 flooding and it is frequently used in the study of viscous fingering [*Zhang et al*., 1997; *Chen and Meiburg*, 1998a, 1998b; *Petitjeans et al*., 1999; *Riaz and Meiburg*, 2004; *Juanes and Lie*, 2008]. It is also relevant during pump-and-treat remediation [*Satkin and Bedient*, 1988]. The five spot pattern is defined by five wells, e.g., four injectors on the corners and one producer in the center (Figure 1a). The symmetry of the flow allows us to investigate the transport process by modeling only a quarter of the full pattern. The quarter five spot pattern is defined with an injector and a producer at the opposite corners of a 2-D domain.

2. Physical and Mathematical Model

2.1. Governing Equations

We consider subsurface transport of a mass of contaminant due to groundwater flow in an aquifer. We model the physical system as two-dimensional Darcy flow of two miscible fluids—water and contaminant—in a porous medium with heterogeneous permeability. We assume that the porous medium has constant porosity ϕ and an isotropic multilognormal stationary random permeability field $k(x,y)=K_g f(\sigma^2_{\ln k}, l)$ characterized by the geometric mean permeability K_g and the permeability correlation function f defined with the log-k variance $\sigma^2_{\ln k}$ and the spatially isotropic correlation length l (Figure 1b). We choose the modified exponential autocovariance function [*Gelhar and Axness*, 1983] to define our permeability correlation function. The two fluids, which are assumed to be first-contact miscible, conservative (nonreactive), neutrally buoyant, and incompressible, have different viscosities—the dynamic viscosity of water is denoted as μ_1 and that of the contaminant is denoted as μ_2. The ratio of the viscosities is denoted as $M=\mu_2/\mu_1$. The diffusivity D between the two fluids is assumed to be constant, isotropic, and independent of the contaminant concentration. We consider the quarter five spot displacement pattern as our flow configuration with the

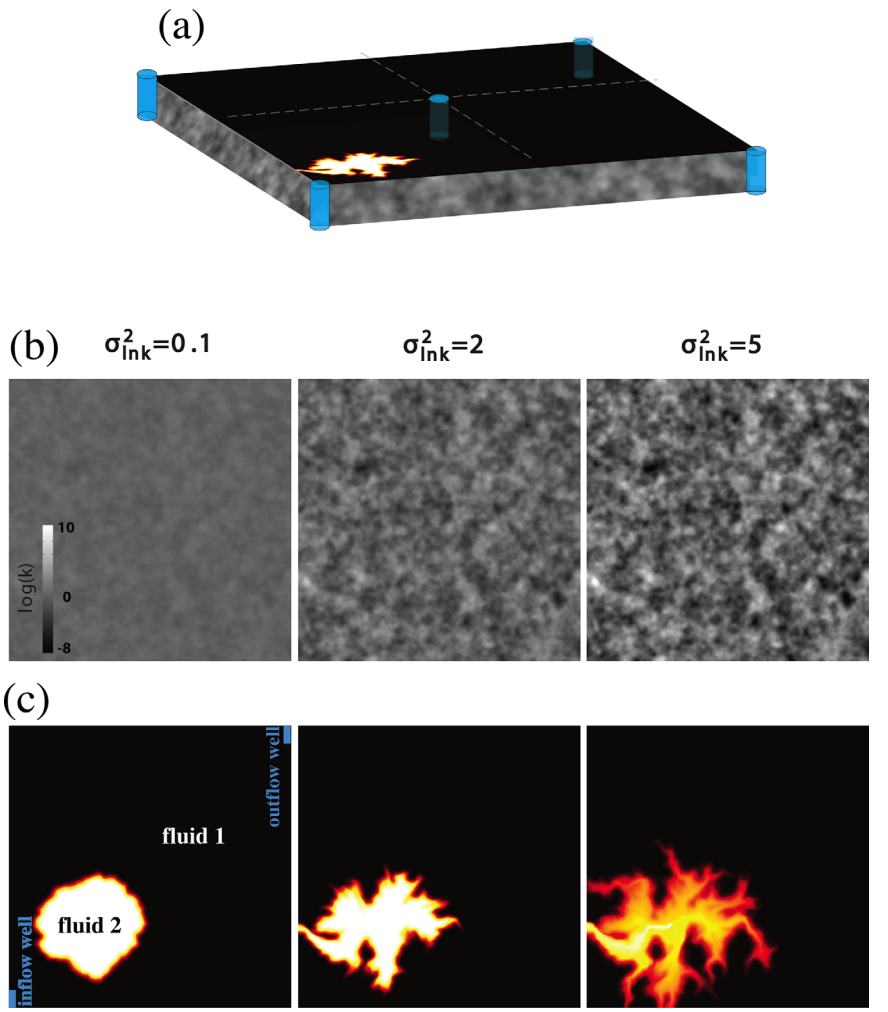

Figure 1. The physical model of flow and transport of a contaminant (fluid 2) through a heterogeneous aquifer in presence of groundwater (fluid 1) flow driven by wells. (a) The five spot flow configuration with four injection wells at the corners and one pumping well at the center. (b) The three multilognormal isotropic permeability fields, $k(x, y)$, used in the current study. The strength of heterogeneity, as given by $\sigma^2_{\ln k}$, increases from left to right. The correlation length is $I = 0.01$. (c) The quarter five spot pattern as our 2-D model domain with injection and pumping wells at opposite corners, and no-flow boundary conditions on all sides. From left to right, initial concentration fields generated for three permeability fields by simulating point injection of a prescribed mass of the contaminant in an unbounded aquifer with the given permeability field. The mass of contaminant is the same for the three initial conditions. As the heterogeneity increases, the initial distribution of the contaminant becomes more irregular.

injection well located at the bottom left and the production well located at the top right corner of the domain (Figure 1c, left). The domain is assumed to be a square of length L. The mean flow direction is from the injection well to the production well, with flow rate Q.

The governing equations in dimensional form are as follows [*Bear*, 1972; *Dentz et al*., 2011; *Jha et al*., 2011b]:

$$\phi \frac{\partial c}{\partial t} + \nabla \cdot (\boldsymbol{u}c - D\nabla c) = 0, \tag{1}$$

$$\boldsymbol{u} = -\frac{k}{\mu}\nabla p, \qquad \nabla \cdot \boldsymbol{u} = 0, \tag{2}$$

in $x \in [0, L]$ and $y \in [0, L]$. The first equation above is a linear advection-diffusion transport equation for the contaminant concentration $c(\boldsymbol{x}, t)$. The second equation is Darcy's law, defining the Darcy velocity of the mixture $\boldsymbol{u}(\boldsymbol{x}, t)$, which satisfies the incompressibility constraint. Although we use statistically stationary permeability fields, the velocity field is nonstationary in space and time due to time-dependent mixture viscosity and the radial flow configuration of the quarter five spot. The fluid pressure field is denoted by $p(\boldsymbol{x}, t)$.

The characteristics scales chosen to nondimensionalize the governing equations are as follows: L is the characteristic length, Q is the injection/production flow rate per unit length in the third dimension $[L^2T^{-1}]$, $T=\phi L^2/Q$ is the characteristic time, μ_1 is the characteristic viscosity, K_g is the characteristic permeability value, and $\mu_1 Q/K_g$ is the characteristic pressure drop. With T as the time scale, the dimensionless time in the simulation can be understood as pore volume injected (PVI), i.e., ratio of the injected fluid volume to the pore volume of the domain. Using the same symbols to denote the dimensionless variables, the governing equations in dimensionless form are

$$\frac{\partial c}{\partial t}+\nabla\cdot\left(\boldsymbol{u}c-\frac{1}{\mathrm{Pe}}\nabla c\right)=0, \tag{3}$$

$$\boldsymbol{u}=-\frac{k(x,y)}{\mu(c)}\nabla p, \qquad \nabla\cdot\boldsymbol{u}=0, \tag{4}$$

in $x\in[0,1]$ and $y\in[0,1]$. The dimensionless concentration c varies from 0 in fluid 1 (water) to 1 in fluid 2 (contaminant). The dimensionless viscosity of the mixture $\mu(c)$, is assumed to be an exponential function of the concentration, $\mu(c)=e^{-Rc}$, where $R=\ln M$ [*Petitjeans and Maxworthy*, 1996]. The Péclet number of the flow is defined as $\mathrm{Pe}\equiv Q/D$. The dimensionless governing parameters of the system are: the log-k variance $\sigma^2_{\ln k}$ and correlation length I of the permeability field, the Péclet number Pe, and the log-viscosity ratio R. In this study, we investigate the effect of $\sigma^2_{\ln k}$ and R on transport properties of the contaminant while keeping the other two parameters fixed. We choose a high value of the Péclet number, $\mathrm{Pe}=10000$, and a low value of the correlation length, $I=0.01$, to simulate an advection-dominated flow in a statistically stationary permeability field.

We simulate the quarter five spot flow by applying no-flow boundary conditions on all four boundaries of the domain and a constant flow rate ($Q=1$) between inlet and outlet, similar to the setup in *Cortis et al.* [2004]. The inlet concentration is fixed at $c_{in}=0$, and a natural outflow condition is used at the outlet, i.e., the outward flux of fluid 2 is equal to the extraction rate times the concentration of fluid 2 arriving at the well, $F_{out}(t)=Q\,c_{out}(t)$.

2.2. Initial Conditions

In this article, we are interested in studying the flow and transport of a subsurface contaminant plume of a given mass, after it has reached its stably stratified depth interval in the aquifer. The shape and concentration distribution of the plume at this depth is determined by the heterogeneity of the porous medium, characteristics of the leakage source, and by other physical properties of the contaminant such as density and viscosity.

To achieve a realistic initial distribution of the contaminant, $c_0=c(t=0)$, in a heterogeneous permeability field, we conduct a separate simulation to determine the initial condition. In these simulations, we assume that the physical properties of the contaminant and the resident water are identical. While it is true that the emplacement of the contaminant would be affected by viscosity contrast, we use the same initial conditions for all the simulations that share the same permeability field spatial distribution. This allows us to compare and contrast results with different viscosity ratios, R, and heterogeneity, $\sigma^2_{\ln k}$, which is one of our objectives here.

We inject a prescribed mass of the contaminant from a point source at a constant rate in a 2-D aquifer domain with natural outflow boundary conditions and characterized by the given permeability field (Figure 1b). There is one such simulation for each permeability field that we study. Therefore, the shape and concentration distribution of initial plumes is different for different permeability fields (Figure 1b). Since the initial concentration fields are different, the viscous fingering process, which depends on local concentration values, will also be different for different $\sigma^2_{\ln k}$ even if R and Pe are the same.

3. Numerical Simulation

We solve equations (1) and (2) using the finite volume method with the two-point flux approximation (TPFA) for the pressure field, and sixth-order compact finite differences for the concentration field [*Jha et al.*, 2011b]. We advance in time using an explicit third-order Runge-Kutta method. To avoid numerical stability issues due to large changes in velocities associated with point source and sink, we impose the inlet

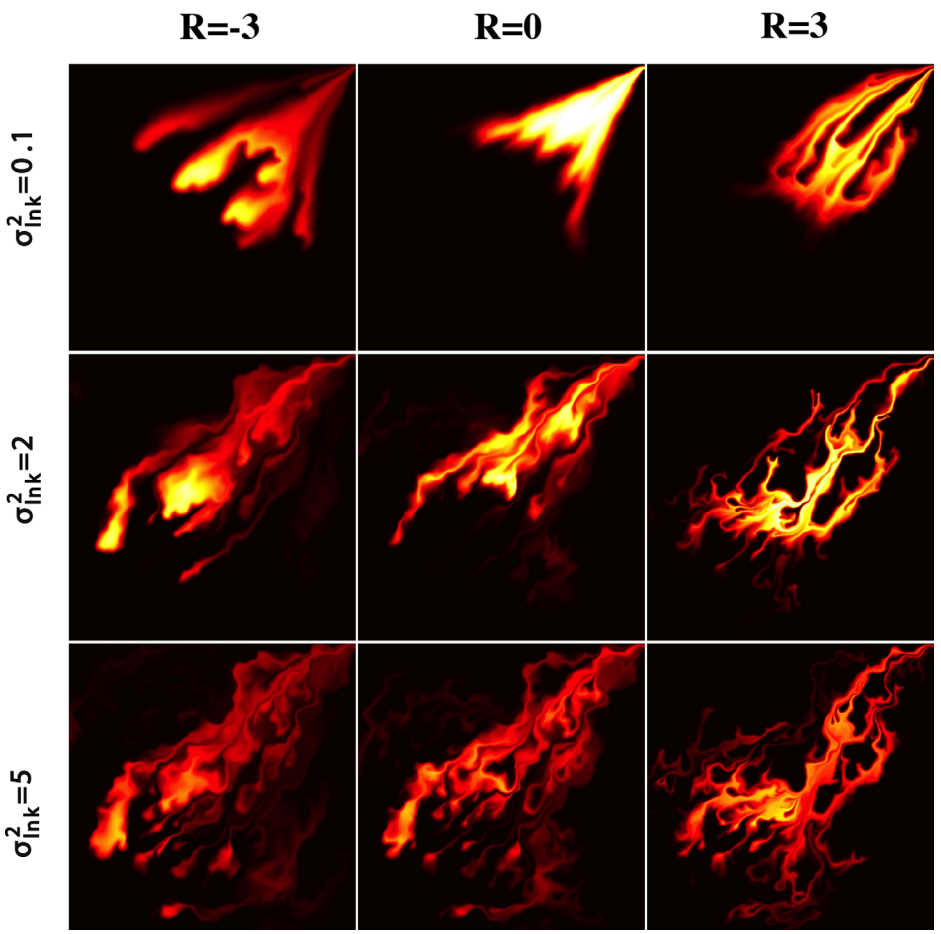

Figure 2. Snapshots of the contaminant concentration field at the time when 20% of the initial mass of contaminant fluid has been removed, for different viscosity contrasts (R) and for different levels of heterogeneity in the permeability field ($\sigma^2_{\ln k}$).

and outlet boundary conditions as line source and sink with length of the line equal to twice the correlation length of the permeability field (Figure 1c).

Because we use heterogeneous permeability fields, it is notoriously difficult to rigorously prove numerical convergence of the simulation results. We have confirmed, however, that the results are insensitive to small variations in the correlation length I, which indicates that the resolution used is sufficient for: (1) resolving the physics from the equations (viscous fingering); and (2) capturing enough length scales of the permeability field in the simulation domain.

In Figure 2, we show the concentration field from typical simulations when 20% of the initial mass of contaminant fluid has been removed, for different viscosity contrasts (R) and for different levels of heterogeneity in the permeability field ($\sigma^2_{\ln k}$). To consider a large range of contaminants encountered during groundwater remediation, we vary the log-viscosity ratio R from -4 to 4, where $R<0$ indicates that the contaminant is more viscous than the aquifer water, and $R>0$ indicates that the contaminant is less viscous than the aquifer water.

The spatial structure of the contaminant plume is very different for $R<0$ and $R>0$. For $R<0$, the resident fluid fingers through the contaminant mass, breaking it up into several smaller islands which then slowly dissolve from their periphery into the resident fluid. This suggests that advection dominates the transport of the contaminant only at early times—even earlier than the breakthrough time—when viscous fingering of the resident fluid breaks up the original contaminant mass. After this time, the small islands of contaminant migrate slowly toward the outlet while fluid mixing is controlled by diffusion across the periphery of these islands.

In contrast, for $R > 0$, viscous fingering at the leading front of the contaminant mass results in stretching and distortion of the original plume, but the entire mass remains connected. Advection dominates over diffusion throughout the displacement by continuous stretching of the interfaces, and it is the removal of the contaminant after breakthrough that is responsible for the eventual loss of strength of viscous fingering.

Heterogeneity affects the spatial structure of the plume in two ways: (a) hold-up of the contaminant in low-permeability or stagnation zones, and (b) fast passage of both fluids through high-permeability pathways. While both hold-up and fast passage lead to spreading of the initial plume, only the latter is responsible for enhanced mixing. Moreover, stagnation zones do not persist at $R > 0$ because of viscous fingering of the contaminant out of these zones.

Finally, it is important to note that even though both high R ($R > 0$) and high $\sigma^2_{\ln k}$ lead to stretching of the interfaces, the two act in distinct ways. In the case of high R, the less viscous contaminant travels faster than the resident fluid and has a tendency to remain segregated inside the fingers, which leads to a high concentration gradient across the stretched interface and subsequently higher mixing in the direction transverse to the interface. Longitudinal mixing across finger tips is small because of the high pressure gradient that maintains the sharpness of the tip. In the case of high $\sigma^2_{\ln k}$, the two fluids share the high-permeability pathways, which promotes longitudinal mixing inside these pathways.

4. Breakthrough and Removal

We quantify the breakthrough and removal behavior of the contaminant plume in our simulations using the first passage time distribution (FPTD), as shown in Figure 3a. We analyze three main features of a FPTD curve: the breakthrough time t_b, the removal time t_r, and the tailing behavior.

It is well known that, as heterogeneity increases, breakthrough occurs earlier and the FPTD has a slower decay in time [*Berkowitz et al.*, 2006; *Le Borgne and Gouze*, 2008], as also observed in Figure 3a. In the case of multiGaussian unconnected permeability fields [*Zinn and Harvey*, 2003], heterogeneity is also related to the observation of lower peak concentrations in the breakthrough curves because heterogeneity leads to enhanced spreading and mixing [*Kapoor and Gelhar*, 1994; *Le Borgne et al.*, 2010]. The role of viscous fingering in early breakthrough of a less viscous plume ($R > 0$) compared to the case of stable displacement ($R \leq 0$), as shown in Figure 3a, is also well known [*Koval*, 1963; *Homsy*, 1987]. However, the interplay between viscosity contrast and heterogeneity remains largely unexplored.

When the strengths of heterogeneity and hydrodynamic instability are comparable, the breakthrough and removal behavior of a plume are determined by the balance between the two effects. Viscous fingering at $R > 0$ leads to an increased variability in the velocities of the contaminant plume, where the dominant fingers travel much faster than the shielded fingers [*Homsy*, 1987]. This variability leads to early breakthrough and broader tailing in the FPTD curves (Figure 3a). The breakthrough concentrations, $c_{out}(t_b)$, are higher because the contaminant arrives at the outlet in the form of well-defined fingers. On the other hand, at $R < 0$, the ambient fluid fingers through the contaminant plume dividing it into smaller plumes, which travel slowly toward the outlet while mixing and diluting continuously from the periphery (Figure 2). The tailing behavior in the FPTD curve is suppressed because of uniformly slow velocities of the divided plume (Figure 3a). The breakthrough concentrations are lower because the contaminant arriving at the outlet is the result of peripheral mixing between the contaminant and the ambient fluid. However, in both $R > 0$ and $R < 0$, viscous fingering leads to fluctuations in the FPTD curve corresponding to episodic arrival of parcels of the contaminant fluid.

We analyze the effect of R and $\sigma^2_{\ln k}$ on the breakthrough time t_b and the removal time t_r from different simulations (Figure 3b). The breakthrough (respectively, removal) time is defined as the time when 0.5% (respectively, 99.5%) of the contaminant has exited the domain. To emphasize the effect of viscosity contrast, i.e., $R \neq 0$, we normalize these two times with t_{b0} and t_{r0}, which are the breakthrough and removal times for $R = 0$ at respective $\sigma^2_{\ln k}$. As R increases from -4 to 4, both the breakthrough time and the removal time decrease because the mixture viscosity $\mu(c)$, which is an exponentially decreasing function of the contaminant concentration, decreases. At very high R, the hydrodynamic effect dominates over the heterogeneity, such that the breakthrough time and the removal time are almost insensitive to the level of heterogeneity. As R decreases, the effect of heterogeneity on t_b and t_r increases because heterogeneity determines the spatial organization of streamlines and the permeabilities of stagnation zones. The effect of heterogeneity is larger on the normalized

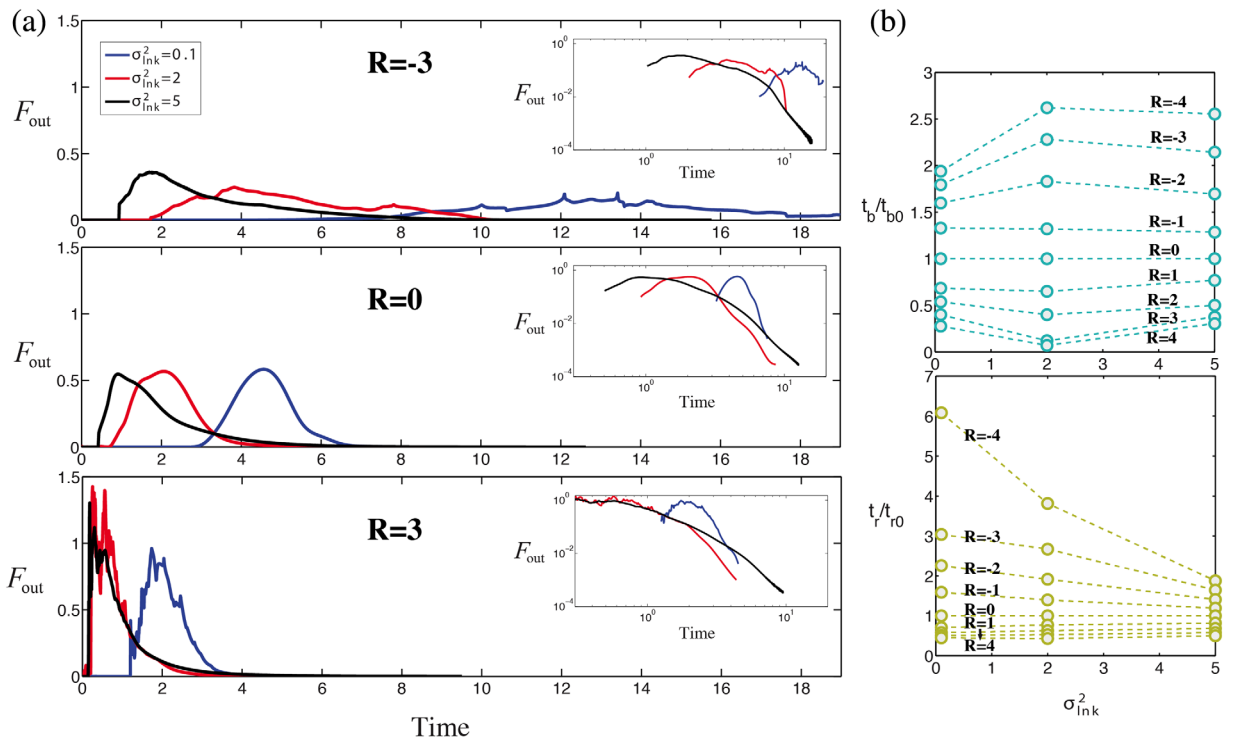

Figure 3. (a) The mass flux of the contaminant (fluid 2) that exits the outflow well as a function of time (the first passage time distribution, or the derivative of the breakthrough curve), for different viscosity contrasts (R), and for different levels of heterogeneity in the permeability field ($\sigma^2_{\ln k}$). Note that each curve corresponds to a single realization of randomly generated permeability field with prescribed $\sigma^2_{\ln k}$. Insets: The late time FPTD in logarithmic scale. Heavy tails of the FPTD that depart from the behavior of homogeneous and equal viscosity case indicate anomalous transport behavior of the contaminant in the system. (b) The breakthrough time (top) and the removal time (bottom) of the contaminant (normalized with respect to the respective values at $R = 0$) as a function of the viscosity contrast and the heterogeneity of the permeability field. Regardless of the heterogeneity level, both the breakthrough time and the removal time decrease as R increases because of increasing mobility of the contaminant. Heterogeneity does not play a significant role in determining the breakthrough time. However, it plays an important role in the removal of a viscous contaminant ($R < 0$) by virtue of contaminant being left stranded in stagnation zones of very low permeability.

removal time t_r/t_{r0} than on the normalized breakthrough time t_b/t_{b0} because the removal process samples a larger fraction of the heterogeneous domain and over a longer duration ($t_r > t_b$) compared to breakthrough, which only samples permeabilities along the breakthrough streamline.

The contaminant concentration at the outlet is related to the mean concentration within the domain. Let $\langle\cdot\rangle$ denote the spatial averaging operator over the domain volume; for instance, $\langle c\rangle$ is the mean concentration in the domain. We derive the evolution equation for the mean concentration by applying the volume averaging operator on the ADE (equation (1)),

$$\frac{d\langle c\rangle}{dt} = F_{in} - F_{out}, \tag{5}$$

Incorporating the boundary conditions at the injection and extraction wells, $F_{in} = 0$ and $F_{out} = Q\,c_{out}$, we obtain the evolution equation for the mean concentration

$$\frac{d\langle c\rangle}{dt} = -Qc_{out}, \tag{6}$$

which states that the mean concentration in the domain decays monotonically with time after breakthrough. Integrating equation (6) in time,

$$\langle c\rangle = \langle c_0\rangle - Q\int_{t_b}^{t} c_{out}\,dt, \tag{7}$$

where the second term on the right-hand side is the cumulative mass (per unit volume) of the contaminant that has flowed out of the domain. Equation (7) explicitly relates the mean concentration to the FPTD curve, $c_{out}(t)$.

Both the breakthrough and the removal time of the contaminant can be determined from the first passage time distribution (FPTD), or its integral, the breakthrough curve (BTC), which is a measure of the cumulative outlet concentration as a function of time. The breakthrough curve is a global measure of disorder in the flow and can be used to characterize the interplay between the effects of viscosity contrast and heterogeneity. As the viscosity contrast between the fluids increases and the medium becomes more heterogeneous, the arrival of contaminant parcels exhibits a wider arrival-time distribution (Figure 3a). It is possible, however, to identify relations between certain features of the FPTD such as the breakthrough and removal times, and changes in the viscosity contrast and the level of heterogeneity. In the next section, we also identify the explicit relation between evolution of mixing and the FPTD, which are related through the evolution of the concentration field.

5. Mixing and Dilution

In groundwater remediation, it is important to have an estimate of the peak concentration of the contaminant and the areal extent of the plume moving through the aquifer, for a given mass of contaminant in the aquifer. Both the peak concentration and spreading of the plume are closely related to the degree of mixing of the contaminant. Mixing can be understood as the decay of fluctuations in the concentration around the perfectly mixed state, i.e., decay of the concentration variance [*Pope*, 2000; *Le Borgne et al*., 2010; *Dentz et al*., 2011; *Jha et al*., 2011a]

$$\sigma^2 \equiv \langle (c - \langle c \rangle)^2 \rangle. \tag{8}$$

We define the degree of mixing χ as follows,

$$\chi \equiv 1 - \frac{\sigma^2}{\sigma^2_{\max}}, \tag{9}$$

where $\sigma^2_{\max} = \langle c_0 \rangle (1 - \langle c_0 \rangle)$ is the maximum variance that corresponds to a perfectly segregated state of the two fluids for a given initial mass (per unit volume of the contaminant), $\langle c_0 \rangle$. In a perfectly mixed state, or when only one of the fluids is present, $\sigma^2 = 0$ and $\chi = 1$.

In Figure 4, we plot the evolution of the degree of mixing with the mass of the contaminant in the aquifer (the contaminant mass-in-place serves as a proxy for time in the post-breakthrough stage). We compare the degree of mixing of a given mass of contaminant for different viscosity contrasts R and heterogeneity levels $\sigma^2_{\ln k}$. The initial values of the degree of mixing at the three levels of heterogeneity are different because of the difference in the initial concentration fields (Figure 1). The vertical profile of the curves at mass-in-place = 1 corresponds to the prebreakthrough stage, i.e., flow during $t < t_b$.

The degree of mixing evolves monotonically from its initial value to the final value $\chi = 1$, when all the contaminant has left the domain. The mixing behavior and the spatial structure of the contaminant plume is very different for $R > 0$ and $R < 0$. In the $R > 0$ case, the contaminant is less viscous and travels faster than the ambient groundwater. This results in an earlier arrival time (Figure 3) and, therefore, an earlier departure of the mixing curve from the vertical line, where the line corresponds to mixing prior to the breakthrough. Viscous fingering initiates at the unstable displacement front, which for $R > 0$, is the downstream front. Viscous fingering leads to significant amount of stretching of the contaminant mass such that "memory" of its initial shape is lost in post breakthrough measurements.

In the $R < 0$ case, it is the upstream front of the contaminant mass that is hydrodynamically unstable. The instability grows more slowly because of the stabilizing effect of the downstream displacement front, which is stable. The contaminant breakthrough is delayed, which results in a higher degree of mixing at the time of breakthrough, however, a smaller rate of mixing after the breakthrough. The contaminant mass disintegrates into small islands, and mixing takes place at the periphery of these islands which forms the interface between the two fluids (Figure 2).

The evolution of mixing is determined by the interplay between viscous fingering (R) and heterogeneity ($\sigma^2_{\ln k}$). For the mildly heterogeneous case ($\sigma^2_{\ln k} = 0.1$), viscous fingering is the main source of disorder in the flow, and therefore the degree of mixing increases for $|R| > 0$. For $\sigma^2_{\ln k} > 0.1$, heterogeneity enhances the degree of mixing by providing high permeability pathways which are shared by both the fluids and lead to stretching of

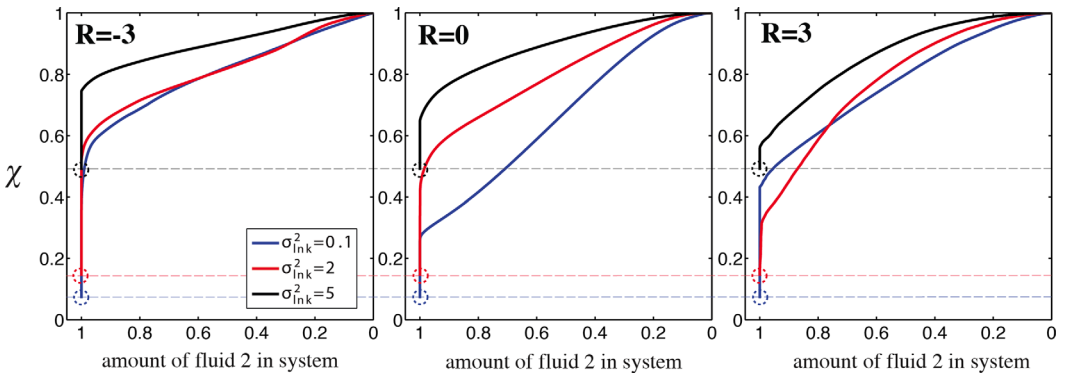

Figure 4. The degree of mixing, χ, as a function of the amount of fluid 2 remaining in the system for different cases of viscosity contrast as well as for different permeability heterogeneities. These curves highlight the evolution of mixing in the post breakthrough stage as the mass is constant (= 1) before the breakthrough. Higher heterogeneity leads to enhanced mixing at early times and this effect decreases as the contaminant is removed. Comparing $R = 0$ with $|R|=3$, the effect of heterogeneity on evolution of the degree of mixing is diminished as the viscosity contrast increases to $|R|=3$. Compared to $R = 0$, $R < 0$ takes longer to break through (Figure 3a) and, therefore, shows higher degree of mixing immediately after breakthrough. In contrast, $R > 0$ results in a lower degree of mixing at breakthrough.

interfaces. However, this effect is modified by the dynamics of viscous fingering, especially when viscosity contrast and permeability heterogeneity are comparable in strength, e.g., $R=\pm 3$ and $\sigma^2_{\ln k}=2$.

To better understand the evolution of the degree of mixing, we derive the theoretical expressions that govern the time dependence of χ. Multiplying the ADE (equation (1)) by the concentration c, applying the volume averaging operator, and incorporating the boundary conditions at the wells, we obtain

$$\frac{d\langle c^2\rangle}{dt} = -\frac{2}{\mathrm{Pe}}\langle|\nabla c|^2\rangle - 2Qc^2_{out}. \tag{10}$$

Differentiating equation (8) with respect to time

$$\frac{d\sigma^2}{dt} = \frac{d\langle c^2\rangle}{dt} - 2\langle c\rangle\frac{d\langle c\rangle}{dt}. \tag{11}$$

Substituting from equations (6) and (10), we obtain the evolution equation for the concentration variance

$$\frac{d\sigma^2}{dt} = -2\epsilon + 2Qc_{out}(\langle c\rangle - c_{out}), \tag{12}$$

where we have defined the mean scalar dissipation rate as $\epsilon \equiv \frac{1}{\mathrm{Pe}}\langle|\nabla c|^2\rangle$ [*Pope*, 2000; *Jha et al*., 2011a]; ϵ is a measure of the rate of mixing based on the amount of fluid-fluid interfacial area available for diffusion.

The evolution equation of ϵ can be obtained by applying the gradient operator to the ADE, taking a dot product with $\boldsymbol{g} \equiv \nabla c$, and applying the averaging operator [*Jha et al*., 2011b],

$$\frac{d\epsilon}{dt} = -\frac{2}{\mathrm{Pe}}\langle\nabla\boldsymbol{u} : \boldsymbol{g}\otimes\boldsymbol{g}\rangle - \frac{2}{\mathrm{Pe}^2}\langle\nabla\boldsymbol{g} : \nabla\boldsymbol{g}\rangle, \tag{13}$$

where $\otimes$ denotes a dyadic product of two vectors resulting in a second-order tensor, and : denotes double contraction. In the derivation of equation (13), we have used the condition of perfectly mixed fluids at the inlet and outlet, i.e., $\boldsymbol{g}_{in}=\boldsymbol{g}_{out}=\boldsymbol{0}$.

From equation (12), the evolution of the concentration variance σ^2, and therefore the degree of mixing χ, is determined by two parts: mixing inside the domain and removal of contaminant mass. The former is related to the evolution of fluid interfaces inside the domain, i.e., evolution of ϵ given by equation (13), and the latter is related to the FPTD, i.e., the evolution of c_{out}.

In Figure 5, we plot the evolution of these two components. Since ϵ is always positive, the first term on the right-hand side of equation (12) acts as a sink term, which means that the fluid-fluid diffusive interface, present due to the initial condition and the disorder in the flow, always enhances mixing. However, in the case of $R > 0$, ϵ rises to higher values compared to the case of $R < 0$, because of fingering-driven stretching of the contaminant mass.

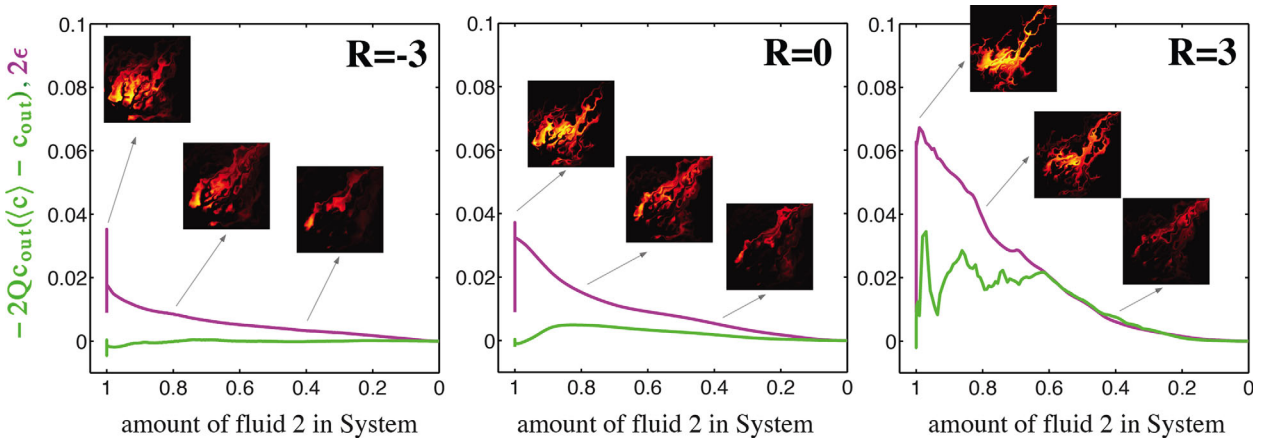

Figure 5. The two contributions to the rate of mixing (equation (12))—the stretching component (ϵ) and the removal component $c_{out}(c_{out}-\langle c\rangle)$—as a function of the amount of fluid 2 remaining in the system for different viscosity contrasts and for the very heterogeneous permeability field ($\sigma^2_{\ln k}=5$). The rate of mixing is the sum of these two components, and it increases with R. Viscous fingering of the contaminant at $R>0$ leads to episodic arrival of the contaminant at the outlet, and consequently, fluctuations in the removal component at $R=3$. For $R\leq 0$, the maximum rate of mixing is achieved before the breakthrough, when ϵ is highest and the removal component is zero ($c_{out}=0$ for $t<t_b$). For $R=3$, the maximum rate of mixing is achieved shortly after the breakthrough, when both ϵ and the removal component are at their maximum. Viscous fingering at $R>0$ leads to enhanced mixing rate in two ways: it enhances ϵ by interface stretching, and it enhances the removal component due to higher c_{out} of the fingers arriving at the outlet.

The second term in equation (12) is the result of the outflow boundary condition. It is completely determined from the FPTD (using equation (7)), and it is zero until breakthrough. After breakthrough, it acts as a source of concentration variance, or scalar energy, when $c_{out}<\langle c\rangle$. This leads to a decline in the rate of increase in mixing from its prebreakthrough value. However, c_{out} may increase with time, for example, when parcels of unmixed contaminant fluid arrive at the outlet during viscous fingering-dominated flow at $R>0$. Since $\langle c\rangle$ continuously decreases with time, the second term in equation (12) can also act as a sink of scalar energy. In other words, removal of the contaminant leads to an increase in the degree of mixing inside the domain. At late times, both ϵ and $\langle c\rangle$ become very small and the degree of mixing slowly increases toward 1 as the contaminant leaves the domain.

6. Impact of Velocity-Dependent Dispersion

We have investigated the impact of hydrodynamic dispersion on unstable displacements in heterogeneous porous media. Geologic porous media are heterogeneous at all scales. Velocity fluctuations due to subgrid-scale heterogeneity enhance local mixing and spreading, and may be incorporated into a Darcy-scale formulation through a velocity-dependent dispersion tensor. Mathematically, the isotropic diffusion tensor in the transport equation is replaced by an anisotropic diffusion-dispersion tensor [*Bear*, 1972]. Hence, our model equations read

$$\phi\frac{\partial c}{\partial t}+\nabla\cdot(\boldsymbol{u}c)-\nabla\cdot(\mathbf{D}\nabla c)=0, \tag{14}$$

$$\boldsymbol{u}=-\frac{k}{\mu}\nabla p, \qquad \nabla\cdot\boldsymbol{u}=0, \tag{15}$$

where the diffusion-dispersion tensor, **D**, is given by

$$\mathbf{D}=\phi D_m\mathbf{I}+\mathbf{D}_u, \tag{16}$$

In the above expression, D_m is the molecular diffusion coefficient, **I** is the unit tensor, and we adopt the following classic formulation of the hydrodynamic dispersion tensor, $\mathbf{D}_u$ [*Bear*, 1972]:

$$D_{u,ij}=\alpha_T\|\boldsymbol{u}\|\delta_{ij}+(\alpha_L-\alpha_T)\frac{u_iu_j}{\|\boldsymbol{u}\|} \quad (i,j=x,y), \tag{17}$$

where α_L and α_T are the longitudinal and transverse dispersivities, respectively. Dispersion is characterized by the following two dimensionless numbers [*Abarca et al.*, 2007; *Hidalgo and Carrera*, 2009]:

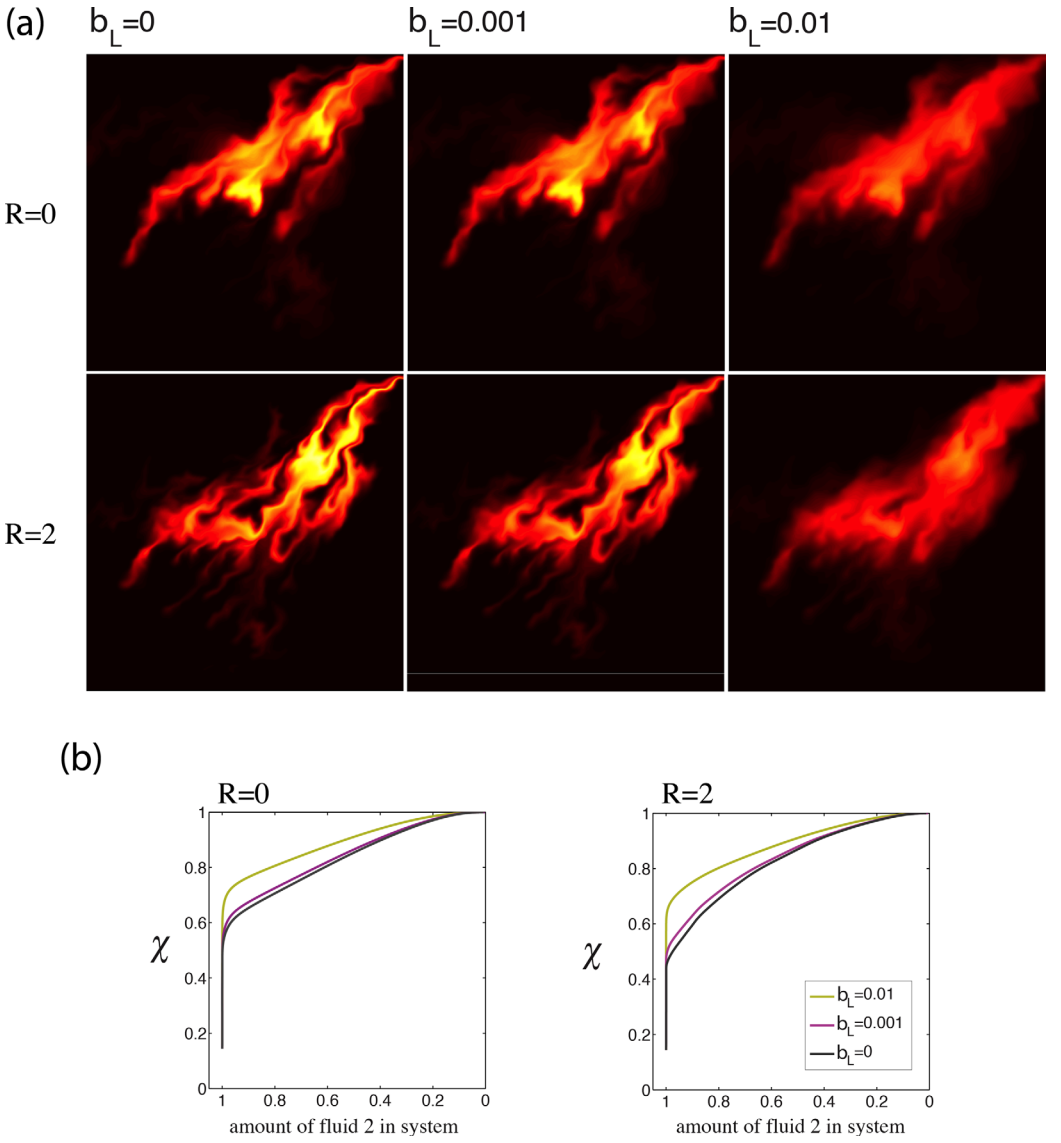

Figure 6. (a) Snapshots of the contaminant concentration field at the time when 20% of the initial mass of contaminant fluid has been removed, for different viscosity contrasts ($R = 0$ and $R = 2$) for the case when we ignore velocity-depended dispersion ($b_L = 0$) and for the case when we consider velocity-depended dispersion with $b_L = 0.001$ ($r_T = 0.1$) and $b_L = 0.01$ ($r_T = 0.1$). (b) The degree of mixing, χ, as a function of the amount of fluid 2 remaining in the system for different viscosity contrasts ($R = 0$ and $R = 2$) for the case when we ignore velocity-depended dispersion ($b_L = 0$) and for the case when we consider velocity-depended dispersion with $b_L = 0.001$ ($r_T = 0.1$) and $b_L = 0.01$ ($r_T = 0.1$). In these simulations, we use multilognormal random permeability field with log-variance $\sigma^2_{\ln k} = 2$ and correlation length $l_x = l_y = 0.01$.

$$b_L = \frac{\alpha_L}{L} \quad \text{and} \quad r_T = \frac{\alpha_T}{\alpha_L}. \tag{18}$$

The parameter b_L plays the role of an inverse Péclet number associated with the dispersion, while r_T measures the strength of anisotropy due to longitudinal and transverse dispersion.

Dispersion enhances mixing in miscible displacements, but does not seem to overwhelm viscous fingering, at least for moderate values of b_L (Figures 6 and 7). The signature of channelized flow due to fingering can be identified in the time evolution of the mass flux out of the domain, as well as in the breakthrough and removal times (Figure 7). The profiles in the case with fingering retain their strong skewness toward earlier arrival of contaminant mass at the outlet.

We have also conducted simulations with variable porosity fields: (1) a multilognormal heterogeneous porosity field with, log-variance $\sigma^2_{\ln \phi} = 2$, and correlation length $l_x = l_y = 0.01$, *fully correlated* with the

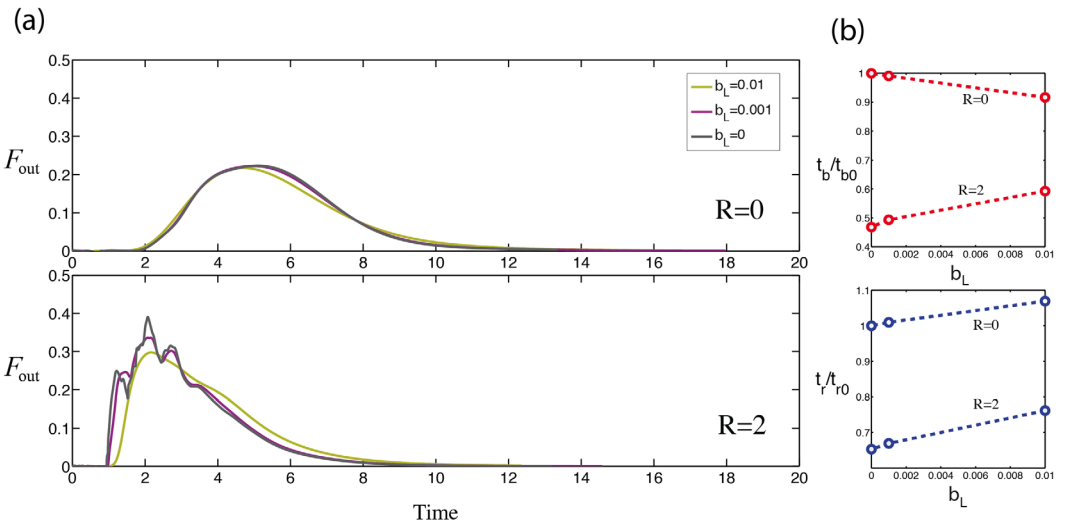

Figure 7. (a) The flux of the contaminant (fluid 2) that exits the outflow well as a function of time (the first passage time distribution, or the derivative of the breakthrough curve), for different viscosity contrasts ($R = 0$ and $R = 2$) for the case when we ignore velocity-depended dispersion ($b_L = 0$) and for the case when we consider velocity-depended dispersion with $b_L = 0.001$ ($r_T = 0.1$) and $b_L = 0.01$ ($r_T = 0.1$). (b) The breakthrough time (top) and the removal time (bottom) of the contaminant (normalized with respect to the respective values at $R = 0$ and $b_L = 0$) as a function of b_L.

permeability field; and (2) multilognormal heterogeneous porosity field with, log-variance $\sigma^2_{\ln \varphi} = 2$ and correlation length $l_x = l_y = 0.01$ that is *uncorrelated* with the permeability field. We have confirmed that both the breakthrough behavior and the evolution of mixing in these simulations with variable porosity are very similar to those in a uniform porosity case.

7. Conclusions

In this paper, we have investigated the impact of viscosity contrast and permeability heterogeneity on mixing and dilution of a contaminant migrating through an aquifer. Using high-resolution simulations, we have identified the key physical mechanisms that control contaminant breakthrough and removal times as well as the evolution of the degree of mixing during transport.

In particular, we have shown that the viscosity contrast between the contaminant and the ambient fluid exerts an important control on the spatial structure of the contaminant plume, and that this in turn plays a dominant role during groundwater cleanup. When the contaminant is less viscous, it has a finger-like structure that remains connected as it travels toward the outlet. In contrast, when the contaminant is more viscous, the plume disintegrates into several smaller plumes. This effect of viscosity contrast on plume structure has a first-order impact on the mixing and dilution of the contaminant, which will influence its rate of biodegradation and the spatial distribution of reaction products.

We have analyzed the impact of velocity-dependent dispersion on the displacement patterns and macroscopic features of transport. Dispersion enhances mixing, but the miscible displacements retain the signature of channelized flow due to fingering in the breakthrough and removal times: strong skewness toward earlier arrival of contaminant mass at the outlet.

Our results suggest that, in a pump-and-treat remediation strategy, viscous fingering of the contaminant leads to enhanced rate of mixing as a result of two mechanisms: increase of the mean scalar dissipation rate by interface stretching, and expedited removal of scalar energy (variance of concentration) from the flow domain. The identification of these physical mechanisms paves the way for combining the individual effects of the two sources of disorder—viscosity contrast and permeability heterogeneity—into a macroscopic model for evolution of mixing during contaminant transport in heterogeneous aquifers.

Acknowledgments
The permeability fields used in the simulations can be downloaded at http://juanesgroup.mit.edu/publications/vfhet. This work was funded by the U.S. Department of Energy through a DOE CAREER Award (grant DE-SC0003907) and a DOE Mathematical Multifaceted Integrated Capability Center (grant DE-SC0009286). Additional funding was provided by an MIT Vergottis Graduate Fellowship (to C.N.).

References

Abarca, E., J. Carrera, X. Sanchez-Vila, and M. Dentz (2007), Anisotropic dispersive Henry problem, *Adv. Water Resour.*, *30*, 913–926.

Bacri, J. C., N. Rakotomalala, D. Salin, and R. Woumeni (1992), Miscible viscous fingering: Experiments versus continuum approach, *Phys. Fluids*, *4*, 1611–1619.
Bear, J. (1972), *Dynamics of Fluids in Porous Media*, pp. 77–616, Elsevier, N. Y.
Bensimon, D., L. P. Kadanoff, S. Liang, B. I. Shraiman, and C. Tang (1986), Viscous flow in two dimensions, *Rev. Mod. Phys.*, *58*, 977–999.
Berkowitz, B., A. Cortis, M. Dentz, and H. Scher (2006), Modeling non-Fickian transport in geological formations as a continuous time random walk, *Rev. Geophys.*, *44*, RG2003, doi:10.1029/2005RG000178.
Boulding, J. R. (1996), *EPA Environmental Assessment Sourcebook*, pp. 113–175, Ann Arbor Press, Chelsea, Mich.
Chen, C. Y., and E. Meiburg (1998a), Miscible porous media displacements in the quarter five-spot configuration. Part 1. The homogeneous case, *J. Fluid Mech.*, *371*, 233–268.
Chen, C. Y., and E. Meiburg (1998b), Miscible porous media displacements in the quarter five-spot configuration. Part 2. Effect of heterogeneities, *J. Fluid Mech.*, *371*, 269–299.
Chen, C.-Y., C.-W. Huang, H. Gadêlha, and J. A. Miranda (2008), Radial viscous fingering in miscible Hele-Shaw flows: A numerical study, *Phys. Rev. E*, *78*, 016306.
Chiogna, G., D. L. Hochstetler, S. Bellin, P. K. Kitanidis, and M. Rolle (2012), Mixing, entropy and reactive solute transport, *Geophys. Res. Lett.*, *39*, L20405, doi:10.1029/2012GL053295.
Christie, M. A. (1989), High-resolution simulation of unstable flows in porous media, *SPE Reservoir Eng.*, *4*, 297–303.
Christie, M. A., and D. J. Bond (1987), Detailed simulation of unstable processes in miscible flooding, *SPE Reservoir Eng.*, *2*, 514–522.
Christie, M. A., A. D. W. Jones, and A. H. Muggeridge (1990), Comparison between laboratory experiments and detailed simulations of unstable miscible displacement influenced by gravity, in *North Sea Oil and Gas Reservoirs II*, edited by J. Kleppe, pp. 37–56, Graham and Trotman, London, U. K.
Cirpka, O. A., R. L. Schwede, J. Luo, and M. Dentz (2008), Concentration statistics for mixing-controlled reactive transport in random heterogeneous media, *J. Contam. Hydrol.*, *98*(1), 61–74.
Cortis, A., C. Gallo, H. Scher, and B. Berkowitz (2004), Numerical simulation of non-fickian transport in geological formations with multiple-scale heterogeneities, *Water Resour. Res.*, *40*, W04209, doi:10.1029/2003WR002750.
Dagan, G. (1989), *Flow and Transport in Porous Formations*, pp. 353–377, Springer, N. Y.
Davies, G. W., A. H. Muggeridge, and A. D. W. Jones (1991), Miscible displacements in a heterogeneous rock: Detailed measurements and accurate predictive simulation, Soc. Pet. Eng., Dallas, Tex., doi:10.2118/22615-MS.
de Anna, P., J. Jimenez-Martinez, H. Tabuteau, R. Turuban, T. Le Borgne, M. Derrien, and Y. Méheust (2013), Mixing and reaction kinetics in porous media: An experimental pore scale quantification, *Environ. Sci. Technol.*, *48*(1), 508–516.
De Wit, A. (2001), Fingering of chemical fronts in porous media, *Phys. Rev. Lett.*, *87*, 054,502.
De Wit, A., and G. M. Homsy (1997a), Viscous fingering in periodically heterogeneous porous media. I. Formulation and linear instability, *J. Chem. Phys.*, *107*, 9609–9618.
De Wit, A., and G. M. Homsy (1997b), Viscous fingering in periodically heterogeneous porous media. II. Numerical simulations, *J. Chem. Phys.*, *107*, 9619–9628.
De Wit, A., and G. M. Homsy (1999), Viscous fingering in reaction-diffusion systems, *J. Chem. Phys.*, *110*, 8663–8675.
De Wit, A., Y. Bertho, and M. Martin (2005), Viscous fingering of miscible slices, *Phys. Fluids*, *17*, 054,114.
Dentz, M., T. Le Borgne, A. Englert, and B. Bijeljic (2011), Mixing, spreading and reaction in heterogeneous media: A brief review, *J. Contam. Hydrol.*, *120*, 1–17.
Dwarakanath, V., K. Kostarelos, G. A. Pope, D. Shotts, and W. H. Wade (1999), Anionic surfactant remediation of soil columns contaminated by nonaqueous phase liquids, *J. Contam. Hydrol.*, *38*, 465–488.
Fernandez, J., and G. M. Homsy (2003), Viscous fingering with chemical reaction: Effect of *in-situ* production of surfactants, *J. Fluid Mech.*, *480*, 267–281.
Fernandez, J., P. Kurowski, P. Petitjeans, and E. Meiburg (2002), Density-driven unstable flows of miscible fluids in a Hele-Shaw cell, *J. Fluid Mech.*, *451*, 239–260.
Flowers, T. C., and J. R. Hunt (2007), Viscous and gravitational contributions to mixing during vertical brine transport in water-saturated porous media, *Water Resour. Res.*, *43*, W01407, doi:10.1029/2005WR004773.
Fu, J.-K., and R. G. Luthy (1986), Aromatic compound solubility in solvent/water mixtures, *J. Environ. Eng.*, *112*, 328–345.
Gelhar, L. W. (1993), *Stochastic Subsurface Hydrology*, pp. 100–200, Prentice Hall, N. Y.
Gelhar, L. W., and C. L. Axness (1983), Three-dimensional stochastic analysis of macrodispersion in aquifers, *Water Resour. Res.*, *19*, 161–180.
Held, R. J., and T. H. Illangasekare (1995), Fingering of dense nonaqueous phase liquids in porous media: 1. Experimental investigation, *Water Resour. Res.*, *31*, 1213–1222.
Hidalgo, J. J., and J. Carrera (2009), Effect of dispersion on the onset of convention during CO_2 sequestration, *J. Fluid Mech.*, *640*, 441–452.
Homsy, G. M. (1987), Viscous fingering in porous media, *Annu. Rev. Fluid Mech.*, *19*, 271–311.
Jha, B., L. Cueto-Felgueroso, and R. Juanes (2011a), Fluid mixing from viscous fingering, *Phys. Rev. Lett.*, *106*, 194,502.
Jha, B., L. Cueto-Felgueroso, and R. Juanes (2011b), Quantifying mixing in viscously unstable porous media flows, *Phys. Rev. E*, *84*, 066,312.
Jha, B., L. Cueto-Felgueroso, and R. Juanes (2013), Synergetic fluid mixing from viscous fingering and alternating injection, *Phys. Rev. Lett.*, *111*, 144,501.
Juanes, R., and K.-A. Lie (2008), Numerical modeling of multiphase first-contact miscible flows. Part 2. Front-tracking/streamline simulation, *Transp. Porous Media*, *72*, 97–120.
Kapoor, V., and L. W. Gelhar (1994), Transport in three-dimensionally heterogeneous aquifers 1. Dynamics of concentration fluctuations, *Water Resour. Res.*, *30*(6), 1775, doi:10.1029/94WR00076.
Kempers, L. J., and H. Haas (1994), The dispersion zone between fluids with different density and viscosity in a heterogeneous porous medium, *J. Fluid Mech.*, *267*, 299–324.
Kitanidis, P. K. (1988), Prediction by the method of moments of transport in heterogeneous formations, *J. Hydrol.*, *102*, 453–473.
Kopf-Sill, A. R., and G. M. Homsy (1988), Nonlinear unstable viscous fingers in Hele-Shaw flows. I. Experiments, *Phys. Fluids*, *31*, 242–249.
Koval, E. J. (1963), A method for predicting the performance of unstable miscible displacements in heterogeneous media, *Soc. Pet. Eng. J.*, *3*, 145–154.
Lajeunesse, E., J. Martin, N. Rakotomalala, and D. Salin (1997), 3D instability of miscible displacements in a Hele-Shaw cell, *Phys. Rev. Lett.*, *79*, 5254–5257.
Le Borgne, T., and P. Gouze (2008), Non-Fickian dispersion in porous media: 2. Model validation from measurements at different scales, *Water Resour. Res.*, *44*, W06427, doi:10.1029/2007WR006279.

Le Borgne, T., M. Dentz, and J. Carrera (2008), Lagrangian statistical model for transport in highly heterogeneous velocity fields, *Phys. Rev. Lett.*, *101*, 090,601.
Le Borgne, T., M. Dentz, D. Bolster, J. Carrera, J.-R. de Dreuzy, and P. Davy (2010), Non-Fickian mixing: Temporal evolution of the scalar dissipation rate in heterogeneous porous media, *Adv. Water Resour.*, *33*, 1468–1475.
Manickam, O., and G. M. Homsy (1995), Fingering instabilities in vertical miscible displacement flows in porous media, *J. Fluid Mech.*, *288*, 75–102.
Mercer, J. W., and R. M. Cohen (1990), A review of immiscible fluids in the subsurface: Properties, models, characterization and remediation, *J. Contam. Hydrol.*, *6*, 107–163.
Mishra, M., M. Martin, and A. De Wit (2007), Miscible viscous fingering with linear adsorption on the porous matrix, *Phys. Fluids*, *19*, 073,101.
Mishra, M., M. Martin, and A. De Wit (2008), Differences in miscible viscous fingering of finite width slices with positive or negative log-mobility ratio, *Phys. Rev. E*, *78*, 066,306.
Mulligan, C. N., R. N. Yong, and B. F. Gibbs (2001), Surfactant-enhanced remediation of contaminated soil: A review, *Eng. Geol.*, *60*, 371–380.
Nagatsu, Y., K. Matsuda, Y. Kato, and Y. Tada (2007), Experimental study on miscible viscous fingering involving viscosity changes induced by variations in chemical species concentrations due to chemical reactions, *J. Fluid Mech.*, *571*, 475–493.
Nicolaides, C., L. Cueto-Felgueroso, and R. Juanes (2010), Anomalous physical transport in complex networks, *Phys. Rev. E*, *82*(5), 055101.
Paterson, L. (1985), Fingering with miscible fluids in a Hele-Shaw cell, *Phys. Fluids*, *28*, 26–30.
Petitjeans, P., and T. Maxworthy (1996), Miscible displacements in capillary tubes. Part 1. Experiments, *J. Fluid Mech.*, *326*, 37–56.
Petitjeans, P., C.-Y. Chen, E. Meiburg, and T. Maxworthy (1999), Miscible quarter five-spot displacements in a Hele-Shaw cell and the role of flow-induced dispersion, *Phys. Fluids*, *11*, 1705–1716.
Pope, S. B. (2000), *Turbulent Flows*, pp. 373–382, Cambridge Univ. Press, Cambridge U. K.
Pritchard, D. (2004), The instability of thermal and fluid fronts during radial injection in a porous medium, *J. Fluid Mech.*, *508*, 133–163.
Riaz, A., and E. Meiburg (2003), Three-dimensional miscible displacement simulations in homogeneous porous media with gravity override, *J. Fluid Mech.*, *494*, 95–117.
Riaz, A., and E. Meiburg (2004), Vorticity interaction mechanisms in variable-viscosity heterogeneous miscible displacements with and without density contrast, *J. Fluid Mech.*, *517*, 1–25.
Rubin, Y. (2003), *Applied Stochastic Hydrogeology*, pp. 200–287, Oxford Univ. Press, N. Y.
Ruith, M., and E. Meiburg (2000), Miscible rectilinear displacements with gravity override. Part 1. Homogeneous porous medium, *J. Fluid Mech.*, *420*, 225–257.
Sajjadi, M., and J. Azaiez (2013), Scaling and unified characterization of flow instabilities in layered heterogeneous porous media, *Phys. Rev. E*, *88*, 033,017.
Satkin, R. L., and P. B. Bedient (1988), Effectiveness of various aquifer restoration schemes under variable hydrogeologic conditions, *Ground Water*, *26*, 488–498.
Tan, C. T., and G. M. Homsy (1988), Simulation of nonlinear viscous fingering in miscible displacement, *Phys. Fluids*, *31*, 1330–1338.
Tan, C.-T., and G. M. Homsy (1992), Viscous fingering with permeability heterogeneity, *Phys. Fluids*, *4*(6), 1089–1993.
Tartakovsky, A. M., G. D. Tartakovsky, and T. D. S. (2009), Effects of incomplete mixing on multicomponent reactive transport, *Adv. Water Resour.*, *32*(11), 1674–1679.
Tchelepi, H. A., and F. M. Orr (1994), Interaction of viscous fingering, permeability heterogeneity and gravity segregation in three dimensions, *SPE Reservoir Eng.*, *9*(4), 266–271.
Tchelepi, H. A., F. M. Orr, N. Rakotomalala, D. Salin, and R. Woumeni (1993), Dispersion, permeability heterogeneity, and viscous fingering: Acoustic experimental-observations and particle-tracking simulations, *Phys. Fluids A*, *5*(7), 1558–1574.
Welty, C., and L. W. Gelhar (1991), Stochastic analysis of the effects of fluid density and viscosity variability on macrodispersion in heterogeneous porous media, *Water Resour. Res.*, *27*, 2061–2075.
Yortsos, Y. C., and M. Zeybek (1988), Dispersion driven instability in miscible displacement in porous media, *Phys. Fluids*, *31*, 3511–3518.
Zhang, H. R., K. S. Sorbie, and N. B. Tsibuklis (1997), Viscous fingering in five-spot experimental porous media: New experimental results and numerical simulation, *Chem. Eng. Sci.*, *52*(1), 37–54.
Zhang, Y.-K., and S. P. Neuman (1990), A quasi-linear theory of non-Fickian and Fickian subsurface dispersion: 2. Application to anisotropic media and the Borden site, *Water Resour. Res.*, *26*, 887–902.
Zimmerman, W. B., and G. M. Homsy (1991), Nonlinear viscous fingering in miscible displacement with anisotropic dispersion, *Phys. Fluids*, *3*(8), 1859–1872.
Zimmerman, W. B., and G. M. Homsy (1992a), Three-dimensional viscous fingering: A numerical study, *Phys. Fluids*, *4*, 1901–1914.
Zimmerman, W. B., and G. M. Homsy (1992b), Viscous fingering in miscible displacements: Unification of effects of viscosity contrast, anisotropic dispersion, and velocity dependence of dispersion on nonlinear finger propagation, *Phys. Fluids*, *4*, 2348–2359.
Zinn, B., and C. F. Harvey (2003), When good statistical models of aquifer heterogeneity go bad: A comparison of flow, dispersion, and mass transfer in connected and multivariate Gaussian hydraulic conductivity fields, *Water Resour. Res.*, *39*(3), 1051, doi:10.1029/2001WR001146.